Planar oxide supported rhodium nanoparticles as model catalysts

Sean M. McClure, M. J. Lundwall, and D. W. Goodman[1]

Department of Chemistry, Texas A and M University, P.O. Box 30012, College Station, TX 77842-3012

Edited by Charles T. Campbell, University of Washington, Seattle, WA, and accepted by the Editorial Board August 21, 2010 (received for review June 8, 2010)

$C_2H_4/CO/H_2$ reaction is investigated on Rh/SiO_2 model catalyst surfaces. Kinetic reactivity and infrared spectroscopic measurements are investigated as a function of Rh particle size under near atmospheric reaction conditions. Results show that propionaldehyde turnover frequency (TOF) (CO insertion pathway) exhibits a maximum activity near $\langle d_p \rangle = 2.5$ nm. Polarization modulation infrared reflection absorption spectroscopy under CO and reaction ($C_2H_4/CO/H_2$) conditions indicate the presence of Rh carbonyl species ($Rh(CO)_2$, Rh(CO)H) on small Rh particles, whereas larger particles appear resistant to dispersion and carbonyl formation. Combined these observations suggest the observed particle size dependence for propionaldehyde production via CO insertion is driven by two factors: (*i*) an increase in propionaldehyde formation on undercoordinated Rh sites and (*ii*) creation of carbonyl hydride species (Rh(CO)H)) on smaller Rh particles, whose presence correlates with the lower activity for propionaldehyde formation for $\langle d_p \rangle < 2.5$ nm.

Ethylene hydroformylation | CO insertion | polarization modulation infrared reflection absorption spectroscopy | Rh/SiO2

A complicating effect of understanding the structure-activity relationships of heterogeneous catalytic reactions at ambient pressures (near 1 atm or above) is the known ability of reactant gas environments to alter the morphology, particle dispersion, and even the types of adsorbates present on certain supported nanoparticle (NP) systems (1–4). For example, elevated pressure CO ambients have been shown to oxidatively disrupt and disperse Rh nanoparticles, creating highly dispersed gem-dicarbonyl species $Rh(CO)_2$ on oxide supports (1–3, 5–8). Under elevated pressure (CO/H_2) and (CO_2/H_2) hydrogenation reaction conditions, Rh(CO)H carbonyl hydride species can also be formed (3, 9–12). The creation and stability of such carbonyl species ($Rh(CO)_2$, Rh(CO)H) can depend on particle size, gas pressure, and surface temperature. The cumulative effect of such factors could potentially have an important effect on the overall catalytic properties of the supported Rh NP surface, especially for catalytic reactions involving surface bound CO. Developing an understanding of how such factors can affect the catalytic properties of supported Rh NPs is important from a fundamental surface chemistry perspective. Unraveling these details will require the ability to conduct spectroscopic and kinetic investigations of an informative probe reaction (*i*) under near atmospheric reaction conditions and (*ii*) on supported Rh nanoparticles surfaces with well defined initial particle size distributions.

CO insertion into adsorbed alkyl groups ($R\text{-}C_xH_y$) to form oxygenates (e.g., alcohols, aldehydes) is an important reaction step in many heterogeneous catalytic reactions. For example, C_2H_4 hydroformylation ($C_2H_4 + CO + H_2$) is a well known reaction for the synthesis of aldehydes via the CO insertion reaction (13). Insightful studies by Chuang and coworkers (14–17) and others (18, 19) have investigated C_2H_4 hydroformylation on oxide supported Rh particles to gain information on the reaction mechanism and reactivity of various adsorbed CO surface species. Motivated by the desire to understand oxygenate reaction pathways in CO hydrogenation catalysis, investigators have utilized C_2H_4 hydroformylation as a probe reaction to understand CO insertion into adsorbed surface ethyl species ($R\text{-}C_2H_5$), without the complications of the CO dissociation step. It has been proposed that propionaldehyde production (CO insertion pathway) proceeds via hydrogenation of adsorbed C_2H_4 to form a surface ethyl species ($R\text{-}C_2H_5$), followed by insertion of adsorbed CO to form an acyl intermediate ($R\text{-}C_2H_5CO$), followed by hydrogenation to form propionaldehyde (C_2H_6CO) (14, 15). Studies of propionaldehyde decomposition on Rh surfaces under ultrahigh vacuum (UHV) conditions, which produces H_2, CO, and ethyl species (along with surface C), also supports these general reaction steps (20). Interestingly, surface coordination of adsorbed CO on Rh also appears to influence its reactivity for CO insertion reactions; for example, linear bound CO appears to be more reactive than CO bound to Rh in a dispersed and/or carbonyl state (e.g., gem-dicarbonyl $Rh(CO)_2$) (16, 19).

The effect of Rh particle size on CO insertion activity has been studied to a lesser extent. Studies of C_2H_4 hydroformylation on cluster derived (19) and traditional (18) Rh powder catalysts have shown that propionaldehyde formation (TOF) is increased as Rh dispersion is increased. Competing ethylene hydrogenation TOF was observed to be structure insensitive over this particle dispersion range in one case (19), but structure sensitive in another study, exhibiting a maximum activity near 4 nm (18). Studies of Rh alloy surfaces (e.g., RhZn (21), RhIr (22), and RhS (23)) have suggested isolated Rh sites on alloy surfaces are favorable for CO insertion under CO hydrogenation or hydroformylation conditions. Combined, these results indicate that undercoordinated and isolated Rh sites on Rh particle surfaces are favorable reaction sites for CO insertion reactions.

Thus, the $C_2H_4 + CO + H_2$ system presents an interesting probe reaction to investigate a surface reaction (CO insertion into adsorbed $R\text{-}C_2H_5$ alkyl groups) whose selectivity, surface adsorbates, and surface morphology can all potentially depend on the initial Rh particle size and the reactant gas conditions. In the present study, we aim to gain insights into the structure-activity relationships of the $CO + C_2H_4 + H_2$ reaction on oxide supported Rh nanoparticle surfaces. Our primary goal is to understand the structure-activity relationships of the CO insertion pathway during C_2H_4 hydroformylation, the underlying reasons driving these structure-activity relationships, and the role of elevated pressure reactant gas in altering the morphology and surface adsorbates present on supported Rh NPs. To accomplish this task we employ well defined Rh/SiO_2 silica model catalyst surfaces (24, 25) to conduct reaction and spectroscopic measurements at elevated pressures (near atm), enabling careful study of the reactivity and selectivity as a function of average Rh particle size. Complementary spectroscopic investigations under ambient

Author contributions: S.M.M., M.J.L., and D.W.G. designed research; S.M.M. and M.J.L. performed research; S.M.M. and M.J.L. contributed new reagents/analytic tools; S.M.M., M.J.L., and D.W.G. analyzed data; and S.M.M. wrote the paper.

The authors declare no conflict of interest.

This article is a PNAS Direct Submission. C.T.C. is a guest editor invited by the Editorial Board.

[1]To whom correspondence should be addressed. E-mail: goodman@mail.chem.tamu.edu.

This article contains supporting information online at www.pnas.org/lookup/suppl/doi:10.1073/pnas.1006635107/-/DCSupplemental.

gas and reaction conditions (polarization modulation infrared (IR) adsorption spectroscopy, PM-IRAS) will enable insights into Rh particle morphology and the state of surface bound CO under reaction conditions as a function of particle size.

Results

Characterization of Rh/SiO_2 Dispersion Under UHV and Near Atmospheric Pressures. Details of Rh/SiO_2 particle size (as determined via scanning tunneling microscopy, STM), active site characterization (24), and percentage of undercoordinated atoms (26) have been discussed in detail in previous investigations. In Fig. 1*A*, we present fraction of undercoordinated atom surface sites ($\leq C_7$ coordinated sites (27)) as a function of Rh NP size based on hard-sphere counting models and STM particle size distribution data (26). C_4H_{10} hydrogenolysis ($C_4H_{10} + H_2 \rightarrow CH_4$, C_2H_6, and C_3H_8) is a well-studied, structure-sensitive reaction (28, 29), which we employ as a probe reaction to correlate STM measurements of Rh NP size at UHV pressures with reactivity measurements at elevated pressures on Rh/SiO_2 surfaces. As shown in previous studies, C_2H_6 selectivity from C_4H_{10} hydrogenolysis is known to be highly favored on undercoordinated surface atoms on Rh metal surfaces (28, 29). Shown in Fig. 1*B* is a plot of C_2H_6 product mol fraction (•) vs. average Rh particle size (nm) ($P_{total} = 210$ Torr). As shown, C_2H_6 product mol fraction sharply increases as average Rh particle size is decreased below $d_p < 5$ nm, exhibiting good correlation between undercoordinated Rh site estimates from STM data based on hard-sphere models (Fig. 1*A*). Additionally, the C_2H_6 selectivity vs. particle size behavior exhibits good qualitative agreement with expectations from technical catalyst studies (28). These characterization results illustrate that Rh particle size estimates obtained via STM measurements under UHV pressures correlate well with elevated pressure kinetic measurements of a well defined probe reaction. Additionally, the particle size behavior of the C_4H_{10} hydrogenolysis reaction (increasing C_2H_6 selectivity with decreasing particle size) will contrast with the Rh particle size dependence observed for the $C_2H_4/CO/H_2$ reaction, where reaction conditions will play a role in altering surface morphology and binding of adsorbed reactants.

C_2H_4 Hydroformylation Reactivity Data. Shown in Fig. 2 is a plot of propionaldehyde TOF vs. average Rh particle size, under standard $C_2H_4/CO/H_2$ reaction conditions at T = 500 K. All reactivity measurements were obtained on freshly prepared Rh/SiO_2 surfaces, to avoid convoluting the data with deactivation effects. Reactivity of a Rh(111) single crystal surface, under identical conditions, is shown by the dotted line. As the data illustrates, a particle size effect is observed, with a maximum in propionaldehyde TOF occurring near an average Rh particle diameter of ~2.5 nm. Overall, Rh/SiO_2 surfaces show nearly an order of magnitude increase in propanal formation when compared to the Rh(111) surface (dotted line).

Additional products present in the product distribution included C_2H_6 (primary competing reaction product) and C_4- hydrocarbon products, along with CH_4, C_3-, and C_5- hydrocarbon products. C_2H_6 production (Fig. S1) on Rh NPs exhibited a higher TOF than planar Rh(111), along with a sharp increase in ethane formation as the size decreased to 1.6 nm. C_2H_6 production then dropped below that observed on 1.6 nm as the average Rh NP size decreased to 1 nm.

CO PM-IRAS Measurements on Rh/SiO_2 Surfaces. To understand the effects of elevated pressure gases on Rh/SiO_2 surface morphology, we begin by examining pure CO IRAS on Rh/SiO_2 as a function of Rh particle size. Shown in Fig. 3 *A–C* are low to elevated pressure CO PM-IRAS measurements obtained on various Rh/SiO_2 surfaces at T = 400 K, as a function of initial Rh particle size. As the data illustrates, low pressure CO IRAS measurements ($P < 5 \times 10^{-6}$ Torr) exhibit CO vibrational features consistent with linear and bridging bound CO on Rh particles, as observed in previous CO IRAS studies on planar (25, 30, 31) and bulk (7, 32) supported Rh surfaces. As P_{CO} is increased at or above $P = 5 \times 10^{-6}$ Torr CO, two additional features (~2,100 cm^{-1} and ~2,040 cm^{-1}) become apparent. These features, which do not exhibit the dipole-dipole coupling shifts with CO pressure observed for linear bound CO, are consistent with Rh gem-dicarbonyl ν_{CO} features ($Rh(CO)_2$, asymmetric, 2,020–2,035 cm^{-1}, and symmetric, ~2,090–2,100 cm^{-1} stretching modes), which have been observed on supported Rh catalysts (2, 5–9, 32, 33). Appearance of these IR features indicate disruption and dispersion of the as-prepared Rh particles by elevated pressures of CO. Fig. 3*D* is a qualitative plot to help visualize the particle size effect of Rh dispersion under elevated CO pressures. This graph plots the intensity of the $I_{Rh(CO)_2,sym}/I_{linear}$ ratio vs. pressure for initial Rh particle sizes. Clearly, a much lower disruptive effect is observed for larger particles under the pure CO conditions probed in Fig. 3, as evidenced by the higher $I_{Rh(CO)_2,sym}/I_{linear}$ ratios observed for small Rh particles (e.g., $\langle d_p \rangle = 1.6$ nm) and the lower $I_{Rh(CO)_2,sym}/I_{linear}$ ratios observed for larger Rh particles (e.g., $\langle d_p \rangle = 3.7$ nm). This observation is qualitatively consistent with previous studies of supported Rh particles on $TiO_2(110)$ (4, 34) and IR studies of Rh/Al_2O_3 supported catalysts (6, 8).

Temperature dependent CO PM-IRAS data (Fig. S2) were also obtained under $P_{CO} = 1$ Torr pressure for the same Rh particle sizes of Fig. 3. As the data of Fig. S2 illustrate, increasing temperature results in a decrease in $Rh(CO)_2$ ν_{CO} features for Rh particles. This observation is consistent with previous studies of supported Rh surfaces under CO environments, which show agglomeration of $Rh(CO)_2$ under increasing temperatures (6, 7, 35). Additionally, this observation is consistent with IRAS studies of Rh NPs supported on planar oxide supports, which demonstrate that at temperatures above T ~ 300 K, Rh atoms can have sufficient mobility to allow dispersed species to agglomerate

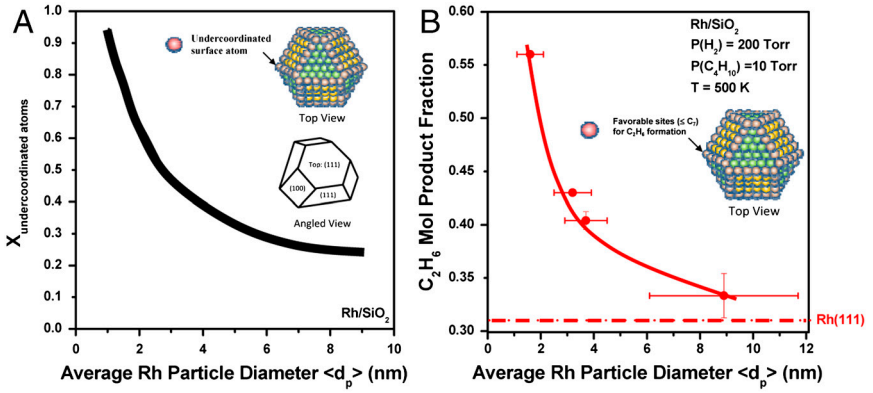

Fig. 1. Rh/SiO_2 particle size characterization: Hard-sphere counting models and C_4H_{10} hydrogenolysis. Fig. 1*A*: Estimates of undercoordinated Rh surfaces sites ($\leq C_7$ coordinated surface atoms) from simple hard-sphere counting models (truncated cuboctahedron particles (26), see inset example). Fig. 1*B*: C_2H_6 mol. fraction from C_4H_{10} hydrogenolysis probe reactions as a function of particle size. Reaction conditions: (T = 500 K, P = 210 Torr, $PH_2:PC_4H_{10} = 20$, and low conversion <2%). Red dashed line shows C_2H_6 mol fraction obtained on a Rh(111) surface under identical conditions.

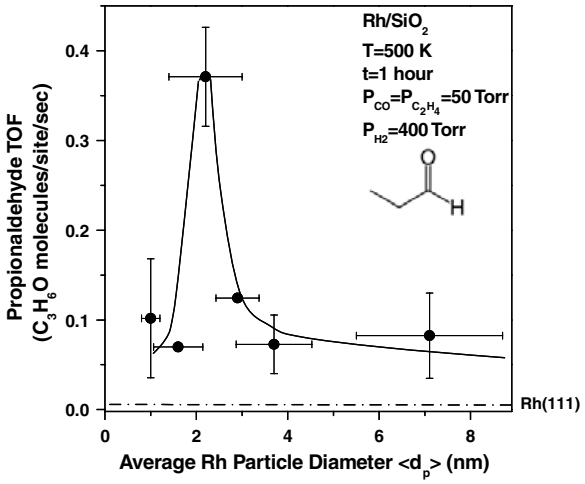

Fig. 2. Propionaldehyde TOF vs. Average Rh Particle Size (nm). Reaction conditions: 50 Torr CO: 50 Torr C_2H_4: 400 Torr H_2 at T = 500 K for 1 h. $\pm\sigma_y$ error bars represent error of repeated reactivity measurements, $\pm\sigma_x$ error bars represent the sigma of the Rh particle size distribution as determined from STM measurements (24). Smooth line present to guide the eye.

to form larger Rh particles (30, 31, 34). Smaller particles appear to maintain dispersed dicarbonyl features at higher temperatures. However, for every temperature (T = 300 K to 600 K) probed, the NP size which shows the clearest resistance to dispersion is $\langle d_p \rangle$ larger than 4 nm, under the $P_{CO} = 1$ Torr conditions.

PM-IRAS Measurements Under $C_2H_4/CO/H_2$ Reaction Conditions. PM-IRAS measurements under reaction conditions (T = 500 K) were obtained as a function of Rh particle size (1.6, 2.9, and 3.7 nm Rh/SiO_2) and are shown in Fig. 4. PM-IRAS measurements were continuously obtained under standard reaction conditions (identical to Fig. 2) every 10 min. For the $\langle d_p \rangle = 2.9$ and 3.7 nm surfaces, under reaction conditions only a single prominent ν_{CO} IRAS feature is observed, one which is consistent with linearly bound CO on Rh. In contrast, IR spectra under reaction conditions on the 1.6 nm surface (particles associated with the decrease in TOF) exhibit *two* prominent ν_{CO} frequencies; one associated with linearly bound CO (2,066 cm^{-1}) and a feature consistent ($\nu_{CO} = 2{,}035$ cm^{-1}) with a Rh carbonyl hydride species (Rh(CO)H) ($\nu_{CO} = 2{,}020$–$2{,}040$ cm^{-1}) (3, 9–12, 36). This species has been observed under CO/H_2 (3) and CO_2/H_2 (10, 12) reaction conditions on dispersed Rh technical catalyst surfaces. Additional PM-IRAS experiments (Fig. S3) were conducted on 1.6 nm Rh/SiO_2 surfaces under CO (50 Torr) and CO/H_2 (50 Torr/400 Torr) environments, which demonstrate the Rh(CO)H ($\nu_{CO} = 2{,}035$ cm^{-1}) feature is present and stable under CO/H_2 as well; IR spectra obtained under the pure CO conditions exhibit the linear and dicarbonyl species displayed in Fig. 3. Efforts to identify IR signals associated with surface ethylene adsorbed species (e.g., ethylidene, ethylidyne) under reaction mixture conditions on the Rh/SiO_2 surfaces were unsuccessful. We suspect this difficulty is likely due to the sensitivity of PM-IRAS for ethylene derived surface species along with the low concentration of these species on Rh coverages below 4 ML (26).

To further probe the nature of Rh carbonyl species under reaction conditions (Rh(CO)H), we conducted additional experiments at a lower reaction temperature (T = 400 K). Shown in Fig. 5 are PM-IRAS spectra taken in an identical procedure as Fig. 4. As the data indicate, under T = 400 K conditions, $Rh(CO)_2$ dicarbonyl features are observed under reaction conditions for nearly an hour, though these features appear to slowly decrease, evidenced by the decrease in intensity of the $Rh(CO)_2$ symmetric stretching feature ($\nu_{CO} = 2{,}105$ cm^{-1}). If the reaction is allowed to continue for an additional hour (60–120 min), the spectra begin to resemble that observed at T = 500 K, a prominent linear bound CO feature and a Rh(CO)H hydride feature. A similar experiment conducted on a larger average Rh particle surface ($\langle d_p \rangle = 2.9$ nm) exhibited a dominant linear bound CO (peak $\nu_{CO} = 2{,}057$ cm^{-1}) (Fig. S4) IR feature throughout the 1 h reaction. The primary observations from the PM-IRAS studies indicate (*i*) correlation between particle size and Rh particle dispersion under pure CO conditions and (*ii*) correlation between the prominent appearance of Rh carbonyl hydride features (Rh(CO)H, $\nu_{CO} = 2{,}035$ cm^{-1}) and the decrease in propionaldehyde activity under reaction conditions as particle size is decreased below 2.5 nm.

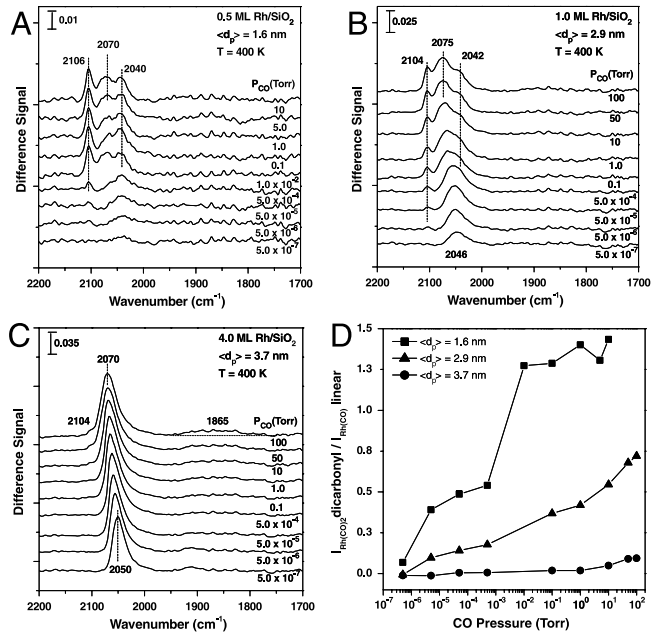

Fig. 3. CO PM-IRAS on Rh/SiO_2 model catalyst surfaces as a function of average Rh particle size from low to elevated CO pressures. Spectra obtained sequentially from low to high CO pressure. Scale bar denotes relative scale between figures. Fig. 3*D*: Ratio of the $Rh(CO)_2$ ν_{CO} stretching intensity to the linear bound ν_{CO} stretching intensity ($I_{Rh(CO)_{2,sym}}/I_{Rh(CO)_{linear}}$) as a function of pressure (Torr) from the data of (*A*–*C*).

Discussion

The reactivity data of Fig. 2, demonstrate that the $C_2H_4/CO/H_2$ reaction is structure sensitive with respect to propionaldehyde (CO insertion) activity, exhibiting a maximum TOF near an average Rh particle size of ~2.5 nm. These two regimes of particle activity ($d < 2.5$ nm and $d > 2.5$ nm), will be discussed separately.

First, we begin by discussing the propionaldehyde activity of the samples as the NP size is decreased from the planar Rh (111) surface to the $\langle d_p \rangle = 2.5$ nm peak TOF. Upon comparison of the Rh(111) propionaldehyde TOF to the largest particle Rh/SiO_2 TOF ($\langle d_p \rangle = 7.1$ nm), we observe a nearly order of magnitude increase in TOF. It is also worthwhile to note that the propionaldehyde TOF observed on Rh(111) ($\sim 5.4 \times 10^{-3}$) is similar in magnitude to a propionaldehyde reactivity measurement (converted to a TOF of $\sim 1 \times 10^{-2}$) conducted over a Rh foil by Somorjai and coworkers (37, 38), under similar reaction conditions. Two factors could contribute to the increased TOF: (1) increase in undercoordinated Rh atoms on dispersed Rh/SiO_2 surfaces going from the close-packed, planar Rh(111) surface to the (7.1 nm) Rh/SiO_2 film and (2) presence of the SiO_2 support. As shown in Fig. 1, an increase in undercoordinated surface atoms should occur going from the close-packed, planar Rh(111) surface to the 7.1 nm Rh/SiO_2 film. However, the small increase

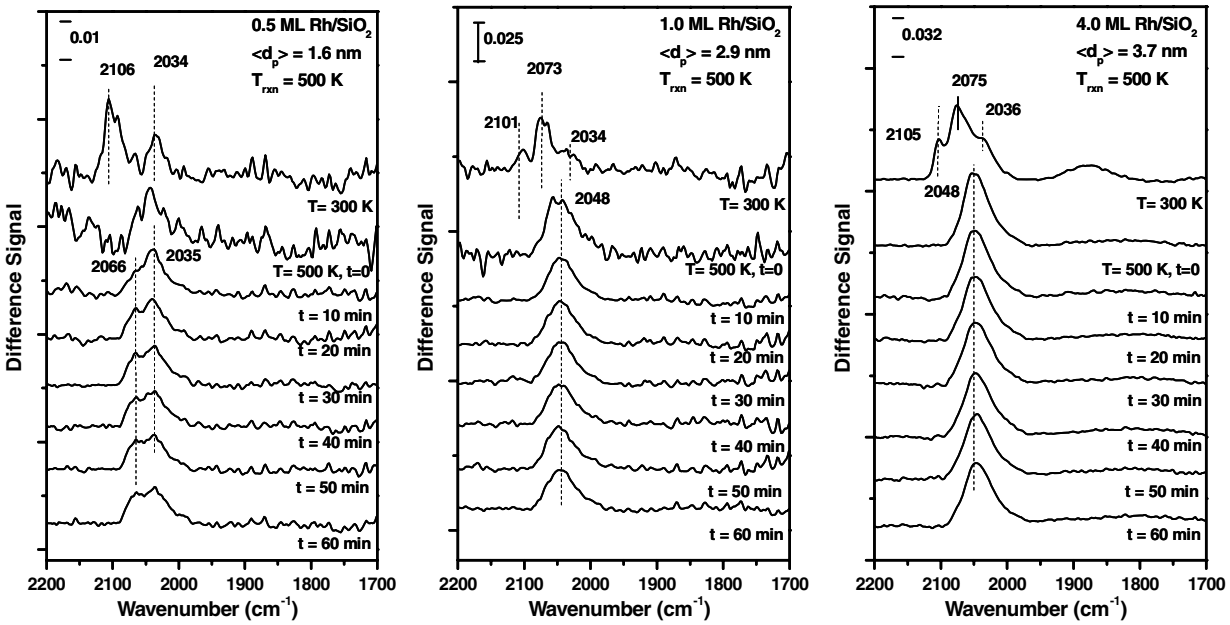

Fig. 4. PM-IRAS on Rh/SiO_2 model catalyst surfaces under reaction conditions (50 Torr CO, 50 Torr C_2H_4, and 400 Torr H_2). Reactant mixtures are introduced at T = 300 K and rapid IR scan (20 scans) is obtained. Sample is then heated to T = 500 K and another rapid IR spectra is obtained (20 scans). Sample is then held at reaction temperature and spectra (692 scans) are obtained every 10 min.

in this concentration expected on such surfaces (~25% from a Rh(111) surface to a 7.1 nm Rh/SiO_2 surface) seems small compared to the nearly order of magnitude difference in CO insertion reactivity. Indeed, in the case of C_4H_{10} hydrogenolysis, C_2H_6 product mol fraction (strongly dependent on undercoordinated Rh sites) is essentially identical for the 7.1 nm (0.33) and Rh(111) surface (0.31) (Fig. 1*B*). Additionally, Rh/SiO_2 characterization measurements (28) indicate that the Rh site density on these two surfaces 7.1 nm (1.3×10^{15} sites/cm^2) and Rh(111) (1.6×10^{15} sites/cm^2), are essentially the same. Combined, these pieces of evidence suggest that the SiO_2 support plays an important role in the CO insertion reaction to form propionaldehyde. This idea is consistent with observations of previous studies (17) indicating hydrogen present on the SiO_2 support may play a role in hydrogenating C_3H_5O acyl groups present on the Rh particle, a reaction step which has been thought to be the rate limiting step in propionaldehyde formation, under certain reaction conditions (14).

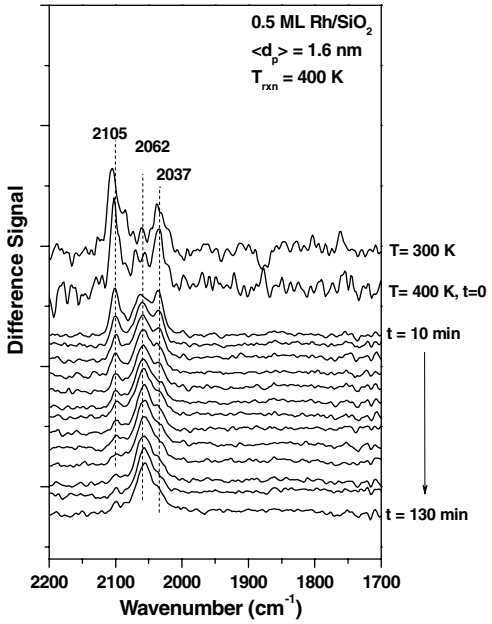

Fig. 5. PM-IRAS on a 1.6 nm Rh/SiO_2 model catalyst surface at T = 400 K under reaction conditions (50 Torr CO, 50 Torr C_2H_4, and 400 Torr H_2). Spectra obtained in an identical fashion to Fig. 4.

As the Rh particle size is decreased from $\langle d_p \rangle = 7.1$ nm to 2.5 nm, a roughly ~5-fold increase in propionaldehyde production (CO insertion activity) is observed. This observation is consistent with the increase in undercoordinated Rh surface sites expected (Fig. 1) from this particle size decrease, which interestingly also exhibit a 5-fold increase in fraction of undercoordinated Rh surfaces sites over this size range. We consider these observations to be strong evidence that propionaldehyde formation occurs more favorably on undercoordinated Rh sites over the $\langle d_p \rangle = 7.1$ nm to 2.5 nm size range. This observation is consistent with and corroborated by previous technical catalyst studies of C_2H_4 hydroformylation on supported Rh catalysts, which show a similar relationship between dispersion and propionaldehyde TOF (18, 19).

However, in the second regime of reactivity (as NP size is decreased below 2.5 nm), a decrease in TOF (CO insertion) is observed. PM-IRAS measurements in pure CO and under reaction conditions help provide information correlating CO insertion activity and CO surface species, as a function of Rh particle size. CO PM-IRAS measurements (Fig. 3) show that disruption and dispersion of Rh particles to form highly dispersed $Rh(CO)_2$ can occur under increasing pure CO pressures. When experiments are conducted as a function of Rh particle size, it becomes readily apparent that in pure CO conditions, particle sizes ~4 nm and above appear to exhibit a resistance to such dispersion, whereas particles below this size are dispersed more readily (Fig. 3*D*). Similar qualitative behavior has been observed on supported catalyst (5, 6, 8) and surface science studies (4, 34) of supported Rh particles, which have demonstrated that larger catalyst loadings (likely associated with larger particles sizes) exhibit resistance to dispersion. Thus, the nature of Rh particle dispersion and CO surface adsorbates under elevated pressures, depend on both initial Rh particle size and CO pressure at a given temperature.

Under $C_2H_4/CO/H_2$ reaction conditions (Fig. 4, T = 500 K) a similar trend is observed. For initial Rh particle sizes above 2.9 nm, PM-IRAS spectra exhibit a single, prominent CO IR feature associated with linearly bound CO. However, for particles below <2.9 nm, *two* prominent CO IR stretching frequencies are observed consistent with both linearly bound CO (2,066 cm^{-1}) and Rh(CO)H carbonyl hydride species (~2,035 cm^{-1}). The key result of the PM-IRAS experiments is that the peak propionaldehyde reactivity is demarcated by differences in CO adsorbates observed in the PM-IRAS spectra; below $d_p \sim 2.9$ nm, prominent features associated with Rh(CO)H and linear bound CO are observed. Above 2.9 nm, only a single, pronounced linear bound CO feature is observed. These data illustrate that changes in Rh particle dispersion and/or changes in CO binding can occur for small Rh particles under reaction conditions at near atmospheric pressures. Data also indicate that surfaces characterized by the presence of Rh(CO)H species appear to be less active for propionaldehyde formation than surfaces containing predominantly linear bound CO on contiguous Rh sites. This observation is consistent with findings on technical catalyst surfaces for C_2H_4 hydroformylation, which has suggested that CO bound to different Rh surface sites show different reactivities for CO insertion. In particular, transient IR measurements by Chuang and coworkers have demonstrated that linear bound Rh is more reactive than CO bound to dispersed, dicarbonyl bound CO ($Rh(CO)_2$) or bridge bound CO (15, 16).

Taken together, the kinetic and spectroscopic data suggest that the observed particle size effect of CO insertion for C_2H_4 hydroformylation on Rh/SiO_2 surfaces is driven by two factors: (1) promotion of CO insertion on undercoordinated Rh surface sites as initial average Rh particle size is decreased to ~2.5 nm (2) decrease in TOF on small Rh particles, which correlates with the presence and formation of Rh(CO)H species under reaction conditions as observed via PM-IRAS. Comparison with Rh(111) reactivity data suggests the SiO_2 support may play a role in the CO insertion reaction on Rh/SiO_2.

One could speculate that CO bound to Rh(CO)H species could be less active for CO insertion for a number of reasons. First, electronic effects could play a role in affecting the insertion reactivity of CO bound to supported Rh(CO)H species. Rh inorganic complexes ($Rh(CO)HL_3$; L = ligand), with tailored ligand constituents, are the catalyst phase utilized in the homogenous catalytic process employed in industry for olefin hydroformylation (13). As it is well known that ligand size and electronic character are critically important variables in determining product selectivity and activity in the homogenous process, it may be that supported Rh(CO)H species also require such ligands to activate the CO bound carbonyl species for high CO insertion activity.

Second, if Rh(CO)H species are highly dispersed like $Rh(CO)_2$ species, geometric constraints could potentially play an inhibiting role for CO insertion on supported Rh(CO)H species compared to surface sites on Rh NPs. While it has been shown via catalytic studies that carefully prepared supported mononuclear Rh (39, 40) and Rh clusters (41) are active for C_2H_4 hydrogenation (39, 41) and ligand exchange ($CO \leftrightarrow C_2H_4$) reactions (39, 40), it may be that Rh atom ensembles or the binding environment present on larger NPs may assist in facilitating the activity of multiadsorbate reactions such as CO insertion.

However, some additional questions remain regarding the extent of dispersity of the Rh/SiO_2 surfaces which produce Rh(CO)H. From previous studies of Rh particles under CO ambients with a multitude of analytical techniques (e.g., EXAFS (1) and IR (5)), it is generally agreed that $Rh(CO)_2$ species are likely associated with highly dispersed Rh species (perhaps small clusters containing ~10's of Rh atoms (1)) present on the oxide support. However, the data regarding the dispersity of Rh(CO)H species remains less clear. STM studies of Rh/TiO_2 surfaces have demonstrated little Rh dispersion under pure H_2 environments (4), and interpretations of IR studies have suggested H_2 hinders oxidative disruption of Rh particles (3) or contributes to agglomeration of $Rh(CO)_2$ species to form larger Rh clusters at higher temperatures (2). However, there certainly appears to be a relationship between $Rh(CO)_2$ and Rh(CO)H, based on the PM-IRAS data under reaction conditions. First, $Rh(CO)_2$ features present under reaction conditions at T = 400 K (Fig. 5) eventually exhibit features consistent with Rh(CO)H at long reaction times. Secondly, Rh particle dispersion under pure CO conditions (Fig. 3) and the presence of the CO insertion reactivity maximum also occur around the same particle size range. The relation between $Rh(CO)_2$ and Rh(CO)H interconversion has also been explored in a previous surface science study of Rh/TiO_2 surfaces by Hayden et al. (42). This study suggested that, under UHV conditions, $Rh(CO)_2$ and Rh(CO)H can interchange under CO and H_2 ambients, respectively. Additional IR studies of supported Rh catalysts have also shown a gradual transition from dicarbonyl IR features to carbonyl hydride features under CO/H_2 environments (11). However, other investigators (2) have argued this observed behavior is simply a transition from $Rh(CO)_2$ species to linearly bound CO on agglomerated Rh particles.

Thus, while the reactivity and spectroscopic data provide evidence suggesting that surface characterized by the presence of Rh(CO)H are less active for the CO insertion reaction, the question of the dispersity of the Rh(CO)H surface under our reaction conditions, and how it compares to the related $Rh(CO)_2$ dispersity remains open. Future measurements, which could measure particle size (e.g., high pressure STM) or Rh-Rh coordination (e.g., EXAFS) under relevant $C_2H_4/CO/H_2$ reaction conditions employed in this study, would be helpful to answering such questions.

In conclusion, the structure-activity behavior of the $C_2H_4/CO/H_2$ reaction was studied as a function of Rh particle size on Rh/SiO_2 model catalyst surfaces, with particular focus on the CO insertion reaction pathway. Kinetic measurements and PM-IRAS spectroscopic techniques were utilized under near atmospheric reaction conditions. Our primary conclusions are as follows:

1. Propionaldehyde (CO insertion) activity under reaction conditions (T = 500 K) showed an optimum Rh particle size of $\langle d_p \rangle \sim 2.5$ nm. Rh/SiO_2 surfaces showed roughly an order of magnitude increase in TOF compared to Rh(111).
2. PM-IRAS measurements under pure CO conditions showed particle disruption and dispersion ($Rh(CO)_2$ formation) from low (5×10^{-7} Torr) to near atmospheric CO pressures. Particle disruption also exhibited a particle size dependence; particles above ~4 nm appeared resistant to CO induced dispersion at elevated pressures; particles below ~4 nm appeared more susceptible to this effect.
3. PM-IRAS under reaction conditions exhibited a particle size dependence in the types of ν_{CO} features observed on the surface. Rh NP sizes (>2.5 nm) above the optimum propionaldehyde TOF exhibited only a single ν_{CO} associated with linearly bound CO. NP sizes below the optimal TOF (<2.5 nm) exhibited ν_{CO} associated with both linearly bound CO and Rh carbonyl hydride CO. PM-IRAS on 1.6 nm particles under reaction conditions at lower temperatures (T = 400 K) exhibited linear and $Rh(CO)_2$ species; PM-IRAS obtained under extended reaction times at T = 400 K eventually produced spectra similar to Rh(CO)H, suggesting a relationship between $Rh(CO)_2$ and Rh(CO)H.
4. Combined, the kinetic and spectroscopic data suggest that the observed particle size effects for CO insertion during C_2H_4 hydroformylation is driven by two factors: (1) promotion of CO insertion on undercoordinated Rh surface sites and (2) decrease in TOF on very small Rh particles, which based

on PM-IRAS measurements under reaction conditions, may be due to the formation of dispersed Rh carbonyl hydride Rh(CO)H species.

Materials and Methods

Experiments were conducted in a coupled UHV surface analysis-elevated pressure reactor/IR cell system described previously (24, 44). Rh/SiO_2 model catalyst surfaces were prepared on molybdenum (Mo) single crystal surfaces, via vapor deposition techniques (24, 45, 46). SiO_2 film thicknesses >5 ML.

For $C_2H_4/CO/H_2$ reactivity measurements, reaction gases were added to the cell at T = 300 K in the following order (*i*) CO, (*ii*) C_2H_4, and (*iii*) H_2 at a ratio of 1:1:8 and a total pressure of 500 Torr; followed by heating to reaction temperature. Product gases from the reactor are sampled at t = 1 hour to determine product formation and TOF values via gas chromatography (GC) (HP 5890, flame ionization (FID) detector) at low conversions (<10% C_2H_4 conversion). Concentrations and retention times of product gases were determined using calibrated hydrocarbon gas mixtures, propionaldehyde, and standard literature FID sensitivity factors and GC techniques (47, 48). Ultrahigh purity (UHP) H_2 was used as received. UHP CO was further purified via heated 4A molecular sieve and LN_2 trapping; UHP C_2H_4 was further purified by multiple freeze pump thaw cycles; C_4H_{10} was further purified via multiple distillations.

PM-IRAS measurements (Bruker Equinox 55) were obtained in a similar UHV/IR cell system (49). PM-IRAS measurements were conducted using 692 scans at a resolution of 4 cm^{-1}, unless otherwise indicated. Background reactivity and PM-IRAS measurements on SiO_2 films showed no activity for reaction or detectable vibrational features across the reaction conditions probed.

ACKNOWLEDGMENTS. We thank Zhen Yan for assistance with the GC setup. We gratefully acknowledge the support of this work by the Department of Energy, Office of Basic Energy Sciences, Division of Chemical Sciences, Geosciences, and Biosciences (DE-FG02-95ER-14511), and the Robert A. Welch Foundation.

1. Van't Blik HFJ, et al. (1983) An extended X-ray absorption fine structure spectroscopy study of a highly dispersed Rh/Al_2O_3 catalyst: the influence of CO chemisorption on the topology of rhodium. *J Phys Chem* 87:2264–2267.
2. Basu P, Panatyotov D, Yates JT, Jr (1988) Rhodium-carbon monoxide surface chemistry: the involvement of surface hydroxyl groups on Al_2O_3 and SiO_2 supports. *J Am Chem Soc* 110:2074–2081.
3. Solymosi F, Pásztor M (1986) Infrared study of the effect of H_2 on CO-induced structural changes in supported Rh. *J Phys Chem* 90:5312–5317.
4. Berkó A, Solymosi F (1999) Adsorption-induced structural changes of Rh supported by $TiO_2(110)$-(1×2): an STM study. *J Catal* 183:91–101.
5. Cavanagh RR, Yates JT, Jr (1981) Site distribution studies of Rh supported on Al_2O_3-an infrared study of chemisorbed CO. *J Chem Phys* 74:4150–4155.
6. Solymosi F, Bánsági T (1993) Low reactivity of rhodium clusters produced in the presence of carbon monoxide. *J Phys Chem* 97:10133–10138.
7. McQuire MW, McQuire GW, Rochester CH (1992) In situ Fourier-transform infrared study of CO-H_2 reactions over Rh/Al_2O_3 catalysts at high pressure and temperature. *J Chem Soc Faraday T* 88:1203–1209.
8. Zaki MI, Kunzmann G, Gates BC, Knözinger H (1986) Highly dispersed rhodium on alumina catalysts: influence of the atmosphere on the state and dispersion of rhodium. *J Phys Chem* 91:1486–1493.
9. Yang AC, Garland CW (1957) Infrared studies of carbon monoxide chemisorbed on rhodium. *J Phys Chem* 61:1504–1512.
10. Henderson MA, Worley SD (1985) An infrared study of the hydrogenation of carbon dioxide on supported rhodium catalysts. *J Phys Chem* 89:1417–1423.
11. Worley SD, Mattson GA, Caudill R (1983) An infrared study of the hydrogenation of carbon monoxide on supported rhodium catalysts. *J Phys Chem* 87:1671–1673.
12. Solymosi F, Erdöhelyi A, Bánsági T (1981) Methanation of CO_2 on supported rhodium catalyst. *J Catal* 68:371–382.
13. Kamer PCJ, Reek JNH, Van Leeuwen PWNM (2002) *Rhodium catalyzed hydroformylation*, eds PWNM Van Leeuwen and C Claver (Kluwer Academic Publishers, New York), pp 35–59.
14. Balakos MW, Chuang SSC (1995) Transient response of propionaldehyde formation during $CO/H_2/C_2H_4$ reaction on Rh/SiO_2. *J Catal* 151:253–265.
15. Chuang SSC, Stevens RW, Jr, Khatri R (2005) Mechanism of C_{2+} oxygenate synthesis on Rh catalysts. *Top Catal* 32:225–232.
16. Chuang SSC, Pien SI (1992) Infrared study of the CO insertion reaction on reduced, oxidized, and sulfided Rh/SiO_2 catalysts. *J Catal* 135:618–634.
17. Chuang SSC, Krishnamurthy R, Tan C-D (1995) Reactivity of adsorbed CO toward C_2H_4, H_2, and NO on the surface of supported rhodium catalysts. *Colloid Surface A* 105:35–46.
18. Hanaoka T, et al. (2000) Ethylene hydroformylation and carbon monoxide hydrogenation over modified and unmodified silica supported rhodium catalysts. *Catalysis Today* 58:271–280.
19. Huang L, et al. (1995) Study in catalysis by carbonyl cluster-derived SiO_2-supported rhodium for ethylene hydroformylation. *Catal Lett* 32:61–81.
20. Brown NF, Barteau MA (1992) Reactions of 1-Propanol and propionaldehyde on Rh (111). *Langmuir* 8:862–869.
21. Sachtler WMH, Ichikawa M (1986) Catalytic site requirements for elementary steps in syngas conversion to oxygenates over promoted rhodium. *J Phys Chem* 90:4752–4758.
22. Fukushima T, Ichikawa M, Matsushita S, Tanaka K, Saito T (1985) Highly selective synthesis of C_2-oxygenates in CO hydrogenation on SiO_2-supported Rh-Ir and Rh-Ti-Ir catalysts. *J Chem Soc Chem Comm* 17:1209–1211.
23. Konishi Y, Ichikawa M, Sachtler WMH (1987) Hydrogenation and hydroformylation with supported rhodium catalysts. Effect of adsorbed sulfur. *J Phys Chem* 91:6286–6291.
24. McClure SM, Lundwall M, Yang F, Zhou Z, Goodman DW (2009) CO oxidation on $Rh/SiO_2/Mo(112)$ model catalysts at elevated pressures. *J Phys Chem C* 113:9688–9697.
25. McClure SM, Lundwall M, Yang F, Zhou Z, Goodman DW (2009) Characterization of active sites on Rh/SiO_2 model catalysts. *J Phys-Condens Mat* 21:1–7.
26. Lundwall M, McClure SM, Goodman DW (2010) Probing terrace and step sites on Pt nanoparticles using CO and ethylene. *J Phys Chem C* 114:7904–7912.
27. Van Hardeveld R, Hartog F (1969) The statistics of surface atoms and surface sites on metal crystals. *Surf Sci* 15:189–230.
28. Kalakkad D, et al. (1993) n-butane hydrogenolysis as a probe of surface sites in rhodium metal particles: correlation with single crystals. *J Phys Chem* 97:1437–1444.
29. Bond GC, Calhoun J, Hooper AD (1996) Hydrogenolysis of propane and n-butane over rhodium catalysts. *J Chem Soc Faraday T* 92:5117–5128.
30. Frank M, Kühnemuth R, Bäumer M, Freund H-J (2000) Vibrational spectroscopy of CO adsorbed on supported ultra-small transition metal particles and single metal atoms. *Surf Sci* 454:968–973.
31. Frank M, Kühnemuth R, Bäumer M, Freund H-J (1999) Oxide-supported Rh particle structure probed with carbon monoxide. *Surf Sci* 427:288–293.
32. Trautmann S, Baerns M (1994) Infrared spectroscopic studies of CO adsorption on rhodium supported by SiO_2, Al_2O_3, and TiO_2. *J Catal* 150:335–344.
33. Yates JT, Jr, Duncan TM, Worley SD, Vaughn RW (1979) Infrared spectra of chemisorbed CO on Rh. *J Chem Phys* 70:1219–1224.
34. Evans J, Hayden B, Mosselmans F, Murray A (1992) Adsorbate induced phase changes of rhodium on $TiO_2(110)$. *Surface Science Letters* 279:L159–L164.
35. Solymosi F, Pásztor M (1985) An infrared study of the influence of CO chemisorption on the topology of supported rhodium. *J Phys Chem* 89:4789–4793.
36. Solymosi M, Pásztor M (1987) Analysis of the IR-spectral behavior of adsorbed CO formed in $H_2 + CO_2$ surface interaction over supported rhodium. *J Catal* 104:312–322.
37. Williams KJ, et al. (1990) Hydrogenation of CO_2, acetone, and CO on a Rh foil promoted by titania overlayers. *Catal Lett* 5:385–394.
38. Williams KJ, Boffa AB, Salmeron M, Bell AT, Somorjai GA (1991) The effects of titania overlayers on $C_2H_4/CO/H_2$ reactions over a Rh foil. *Catal Lett* 11:77–88.
39. Bhirud VA, Ehresmann JO, Kletnieks PW, Haw JF, Gates BC (2006) Rhodium complex with ethylene ligands supported on highly dehydroxylated MgO: synthesis, characterization, and reactivity. *Langmuir* 22:490–496.
40. Ogino I, Gates BC (2010) Reactions of highly uniform zeolite H-b-supported rhodium complexes: transient characterization by infrared and X-ray absorption spectroscopies. *J Phys Chem C* 114:8405–8413.
41. Argo AM, Gates BC (2003) MgO-supported Rh_6 and Ir_6: structural characterization during the catalysis of ethene hydrogenation. *J Phys Chem B* 107:5519–5528.
42. Hayden BE, King A, Newton MA (1997) The reaction of hydrogen with $TiO_2(110)$ supported rhodium gem-dicarbonyl. *Surf Sci* 397:306–313.
43. Zaera F, Somorjai GA (1984) Hydrogenation of ethylene over platinum (111) single-crystal surfaces. *J Am Chem Soc* 106:2288–2293.
44. Szanyi J, Goodman DW (1993) Combined elevated pressure reactor and ultrahigh vacuum surface analysis system. *Rev Sci Instrum* 64:2350–2352.
45. Xu X, Goodman DW (1992) New approach to the preparation of ultrathin silicon dioxide films at low temperatures. *Appl Phys Lett* 61:774–776.
46. Chen MS, Santra AK, Goodman DW (2004) The structure of thin SiO_2 films grown on Mo(112). *Phys Rev B* 69:1–7.
47. Black FM, High LE, Sigsby JE (1975) The application of total hydrocarbon flame ionization detectors to the analysis of hydrocarbon mixtures from motor vehicles, with and without emission control. *Water Air and Soil Poll* 5:53–63.
48. Purnell H (1962) *Gas Chromatography* (John Wiley & Sons, Inc., NY), pp 265–329.
49. Gao F, et al. (2009) CO oxidation on Pt group metals from ultrahigh vacuum to near atmospheric pressures I. rhodium. *J Phys Chem C* 113:182–192.